Theoretical study on the electronic structures and phosphorescent properties of a series of iridium(III) complexes with the different positional N-substitution in the pyridyl moiet...

ARTICLE *in* JOURNAL OF LUMINESCENCE · FEBRUARY 2015

Impact Factor: 2.72 · DOI: 10.1016/j.jlumin.2014.10.064

7 AUTHORS, INCLUDING:

Deming Han
Changchun University of Science and Tech...
30 PUBLICATIONS **98** CITATIONS

SEE PROFILE

Journal of Luminescence 159 (2015) 66–72

Contents lists available at ScienceDirect

Journal of Luminescence

journal homepage: www.elsevier.com/locate/jlumin

Theoretical study on the electronic structures and phosphorescent properties of a series of iridium(III) complexes with the different positional N-substitution in the pyridyl moiety

Deming Han [a], Fengqi Hao [a], Jian Tian [b], Chunying Pang [a], Jingmei Li [a], Lihui Zhao [a,*], Gang Zhang [c]

[a] School of Life Science and Technology, Changchun University of Science and Technology, Changchun 130022, PR China
[b] Clean Energy Technology Laboratory, Changchun University of Science and Technology, Changchun 130022, PR China
[c] State Key Laboratory of Theoretical and Computational Chemistry, Institute of Theoretical Chemistry, Jilin University, Changchun 130023, PR China

ARTICLE INFO

Article history:
Received 21 April 2014
Received in revised form
22 October 2014
Accepted 27 October 2014
Available online 4 November 2014

Keywords:
DFT
TDDFT
Iridium
Phosphorescence
Absorption
Emission

ABSTRACT

The geometry structures, electronic structures, absorption and phosphorescent properties of a series of iridium(III) complexes with the different N-substitution cyclometalating ligand and the same benzyldiphenylphosphine auxiliary ligand have been theoretically investigated by using the density functional theory method. The lowest energy absorption wavelengths are located at 378 nm for **A**, 430 nm for **B**, 411 nm for **C**, 436 nm for **D**, and 394 nm for **E**. The introduction of N atom substitution at 1-, 2-, 3-, and 4-positions on the pyridyl moiety of complex **A** leads to an obvious redshifted absorption. The lowest energy emissions for complexes **A**–**E** are localized at 450, 409, 438, 483, and 429 nm, respectively, simulated in CH_2Cl_2 medium at M052X level. Ionization potential and electron affinity have been calculated to evaluate the injection abilities of holes and electrons into these complexes. For complex **C**, the calculated results showed that it can possibly possess the larger radiative decay rate (k_r) value than those of other four complexes. It is anticipated that the theoretical studies can provide valuable information for designing new phosphorescent metal complexes of organic light-emitting diodes.

1. Introduction

In recent years, many transition metal (such as Ir, Pt, Os, Ru, etc.) complexes have attracted considerable attention as the emitting layers in organic light-emitting diodes (OLEDs) because of their good color purity, high phosphorescence emission quantum yields, short excited triplet state lifetime, and high photochemical stability [1–8]. Especially, phosphorescent Ir(III) complexes have been extensively investigated due to their good phosphorescent emission properties since the pioneering works were performed by Thompson and coworkers [9–11]. Many efforts have been made in the utilization of appropriate iridium(III) complexes and optimization of the device configurations to achieve high efficiency in OLED displays [12–16]. The Ir(III) phosphorescence complexes can harvest both singlet and triplet excitons as light, leading to a theoretical level of unity for internal quantum efficiency in phosphorescent OLEDs and obtaining an efficiency four times higher than fluorescent materials [17–20]. It is known that FIrpic [21,22] and iridium(III) bis(4,6-difluorophenylpyridinato) tetrakis(1-pyrazolyl)-borate (FIr6) [23] have been considered as excellent dopants for greenish-blue and sky-blue PhOLEDs. In fact, there are also several of strategies to tune the emission color or efficiency of the Ir(III) complexes, such as designing new cyclometalating ligands, ancillary ligands, or attaching different substituents [24–27]. It is noted that electron deficient and/or higher field strength L\widehatX ancillaries, such as pyridylazolate and imidodiphosphinate, and phosphorus-containing chelates, such as benzyl phosphine and phosphine substituted pyrazole, are very suitable for the construction of blue- or even bluish-green-emitting Ir(III) metal phosphors [28–31].

Chou et al. have reported a few true blue-emitting Ir(III) phosphors employing benzyldiphenylphosphine as the ancillary chelate [32]. To investigate the influence of substitution on photophysical and spectra properties of these Ir(III) complexes, a series of derivatives by a systematic substitution of the “CH” group by the electron-withdrawing nitrogen (N) atom at 1-, 2-, 3-, and 4-positions on the pyridyl moiety of fppz [5-(2-pyridyl)-3-trifluoromethylpyrazole] ligands in the complex **A** have been theoretically designed and

* Corresponding author.
E-mail address: zhaolihui@yahoo.com (L. Zhao).

http://dx.doi.org/10.1016/j.jlumin.2014.10.064
0022-2313/

studied (Fig. 1a). It is anticipated that these theoretical results can provide useful guidelines for the design and preparation of Ir(III)-based phosphorescent complexes used as the emitters in OLEDs.

2. Computational details

The ground state geometry for each molecule was optimized by the density functional theory (DFT) method with Becke's three parameter hybrid method combined with the Lee–Yang–Parr correlation functional (denoted as B3LYP) [33–35]. The geometry optimizations of the lowest triplet states (T_1) were performed by unrestricted B3LYP approach. The calculated expectation values of total spin $\langle S^2 \rangle$ with $s(s+1)$ have been compared to check the spin contamination, which can be seen that in this work the spin contamination can be neglected due to all the $\langle S^2 \rangle$ values differing from $s(s+1)$ only by 0.53–0.95%.

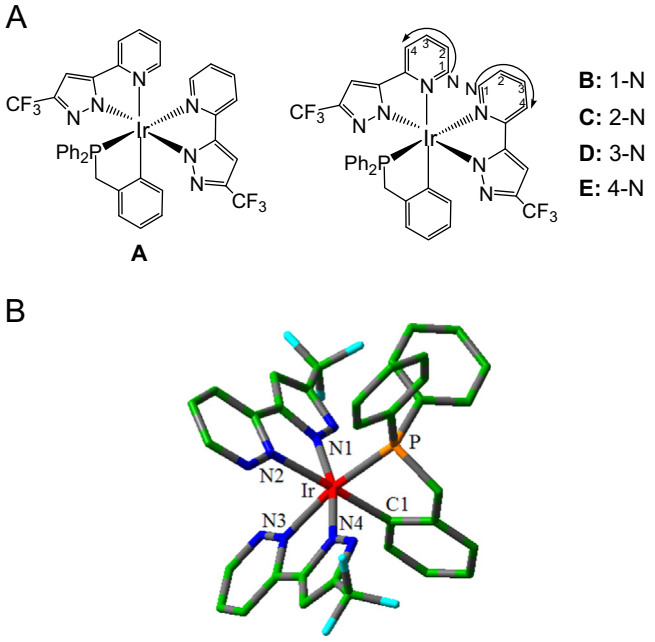

Fig. 1. (a) Sketch map of the structures of iridium(III) complexes **A**, **B**, **C**, **D**, and **E**. (b) Representative optimized structure of complex **B** (H atoms omitted).

On the basis of the ground- and excited-state equilibrium geometries, the time-dependent DFT (TDDFT) approach associated with the polarized continuum model (PCM) in dichloromethane (CH_2Cl_2) medium was applied to investigate the absorption and emission spectral properties, which the random phase approximation (RPA) is implemented herein. The "double-ξ" quality basis set LANL2DZ associated with the pseudopotential was employed on atom Ir [36,37]. The 6-31+G(d) basis set was used for nonmetal atoms in the gradient optimizations. Furthermore, the stable configurations of these complexes can be confirmed by frequency analysis, in which no imaginary frequency was found for all configurations at the energy minima. The frontier molecular orbitals of the ground state complexes were plotted by using the GaussView 5.0.8 software. The absorption spectra are simulated by using the GaussSum 2.5 software [38] with the full width at half-maximum (FWHM) value of 3000 cm^{-1} based on the data obtained via TDDFT calculations. All calculations were performed with the Gaussian 09 software package [39].

3. Results and discussion

3.1. Geometries in the ground state S_0 and triplet excited state T_1

The sketch maps of the five complexes **A–E** (**A–E** indicates **A**, **B**, **C**, **D**, and **E**, the same hereafter) are presented in Fig. 1a, and the optimized ground state geometric structure for **B** is shown in Fig. 1b along with the numbering of some key atoms. The main geometrical parameters in the ground state are summarized in Table 1. All complexes have a distorted octahedral structures around the Ir(III) metal center with d^6 configuration. From Table 1, it can be seen that the systematic substitution of the "CH" group by the N atom on the pyridyl moiety of fppz ligands in complex **A** does not cause obvious changes (<0.015 Å) in the metal–ligand bond distances. In addition, the bond angles and dihedral angles listed in Table 1 for complexes **B**, **C**, **D**, and **E** also show some change with respect to those of complex **A**. The changes of the calculated coordination bond angle are minor (less than 0.8°) from **A** to **B**, **C**, **D**, and **E**.

The calculated geometrical parameters of the lowest lying triplet excited states for these complexes are also listed in Table 1. In addition, the changes of the Ir(III)-related coordination bond lengths between the ground (S_0) and excited state (T_1) for complexes **A–E** are shown in Fig. S1 (Supporting

Table 1
Main optimized geometry parameters for complexes **A**, **B**, **C**, **D**, and **E**.

	A		**B**		**C**		**D**		**E**	
	S_0	T_1	S_0	T_1	S_0	T_1	S_0	T_1	S_0	T_1
Bond length (Å)										
Ir–C1	2.0694	2.0356	2.0643	2.0086	2.0666	2.0219	2.0695	2.0263	2.0677	2.0207
Ir–N1	2.0586	2.0816	2.0547	2.0751	2.0600	2.0957	2.0595	2.0795	2.0597	2.0927
Ir–N2	2.2280	2.2843	2.2285	2.2525	2.2420	2.2976	2.2244	2.2871	2.2302	2.3101
Ir–N3	2.1526	2.1137	2.1378	2.1128	2.1572	2.1175	2.1458	2.1047	2.1532	2.1119
Ir–N4	2.0648	1.9830	2.0575	1.9857	2.0622	1.9639	2.0664	1.9881	2.0675	1.9686
Ir–P	2.3247	2.3553	2.3241	2.3511	2.3228	2.3651	2.3299	2.3624	2.3248	2.3654
Bond angle (deg.)										
N1–Ir–N2	76.59	75.18	76.44	74.82	76.22	74.28	76.61	75.14	76.54	74.32
N3–Ir–N4	77.34	79.48	77.48	78.81	77.17	79.30	77.37	79.21	77.28	79.41
C1–Ir–P	80.49	81.46	81.27	82.56	80.71	81.87	80.40	81.72	80.47	81.44
N1–Ir–N4	167.18	166.94	170.60	168.92	168.69	167.74	167.36	167.13	166.60	165.49
N2–Ir–C1	175.77	172.34	172.43	166.14	174.49	168.54	175.51	171.55	175.74	170.77
N3–Ir–P	172.03	174.45	170.84	173.84	171.81	174.16	171.88	174.83	172.20	175.21
Dihedral angle (deg.)										
N1–N2–N4–C1	8.01	4.68	3.99	1.75	6.11	2.80	8.20	4.66	8.69	4.47
N1–N3–N4–P	9.74	10.39	7.03	6.07	8.59	9.51	9.69	9.71	9.83	10.93
N2–N3–C1–P	5.82	7.97	11.26	15.72	7.91	12.80	6.03	8.74	5.67	9.65

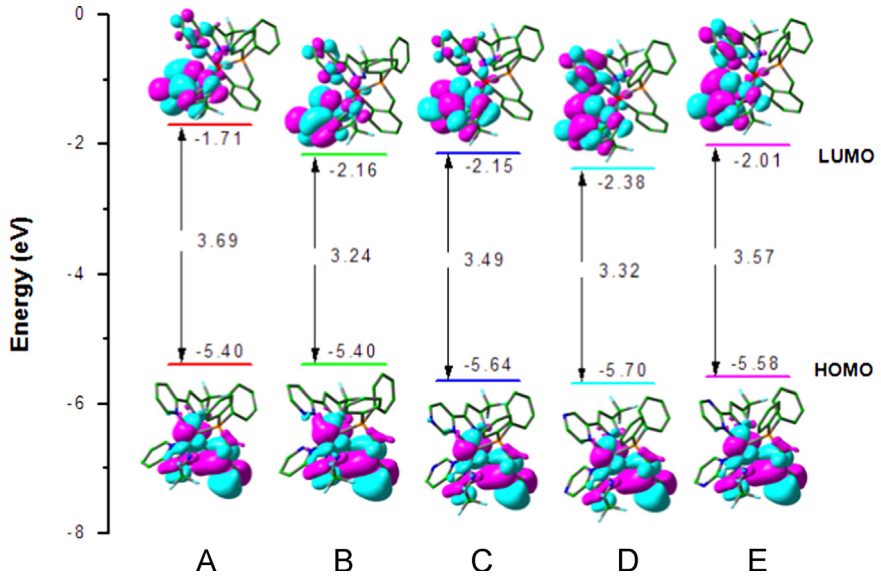

Fig. 2. Presentation of the energy levels, energy gaps, and orbital composition distribution of the HOMO and the LUMO for complexes **A**, **B**, **C**, **D**, and **E**.

information). It can be seen that the Ir–C1, Ir–N3, and Ir–N4 bond lengths are shortened from the S_0 to T_1 excited state, resulting in the strengthened interaction between metal and fppz ligands. Whereas, the Ir–N1, Ir–N2, and Ir–P bond lengths becomes longer from the S_0 to T_1 excited state. In addition, the bond angles of N2–Ir–C1 show a large change ($<7^\circ$) from the S_0 to T_1 excited state. For the stronger interaction between the N^N cyclometalating ligand and the metal Ir(III) in complexes **B**, **C**, **D**, and **E**, the N^N ligand will have the greater effect on the frontier molecular orbitals (FMOs) in both the ground state and the excited state.

3.2. Molecular orbital properties

To further investigate the electronic structure of complexes **A**–**E**, the characters of the HOMO (highest occupied molecular orbital) and LUMO (lowest unoccupied molecular orbital) are analyzed in the subsection. The HOMO and LUMO distribution, energy levels, and energy gaps between of LUMO and HOMO ($\Delta E_{L\to H}$) of complexes **A**–**E** are plotted in Fig. 2. The calculated frontier molecular orbital compositions for **A**–**E** are also listed in Tables S1–S5 (Supporting information).

From Fig. 2, it can be seen that the N substitution on the pyridyl moiety of fppz ligands in the complex **A** does not obviously affect the distribution of the HOMO and LUMO. The electron density of HOMO of all these complexes are mainly localized on the Ir(III) d-orbital (27–29%) and bdp (benzyldiphenylphosphine) auxiliary ligand π-orbital (61–64%), while the LUMO is predominantly contributed by the N^N ligands. It is noted that the introduction of the N substituent at different positions of the pyridyl moiety in N^N ligands has the obvious effect on the energy levels of HOMO and LUMO (shown in Fig. 2). On the whole, the HOMO and LUMO energy levels for complexes **B**, **C**, **D**, and **E** are decreased with respect to those of **A**. In addition, for **B**, **C**, **D**, and **E**, the N substitution stabilizes the LUMO energy levels more evidently than that of the HOMO, which results in a decrease of the HOMO−LUMO energy gap in comparison with that of **A**. This also indicates that the HOMO localized on the Ir(III) and bdp ligands may not be intensely affected by the modification of N^N ligands, while the changes of the LUMO energy levels are obvious for their mostly distribution on the N^N ligands. For example, due to the largely lower LUMO energy level and the reduced HOMO level for complex **D** with the N substitution at the 4-position, the $\Delta E_{L\to H}$ for **D** is decreased by 0.37 eV in comparison to that of complex **A**.

Table 2
The calculated vertical IP (IP_v), adiabatic IP (IP_a), hole extraction potential (HEP), vertical EA (EA_v), and adiabatic EA (EA_a), electron extraction potential (EEP), and reorganization energies for electron ($\lambda_{electron}$) and hole (λ_{hole}), unit: eV.

	IP_v	IP_a	EA_v	EA_a	HEP	EEP	$\lambda_{electron}$	λ_{hole}
A	6.640	6.444	0.485	0.603	6.231	0.725	0.239	0.409
B	6.629	6.415	0.904	1.051	6.190	1.198	0.294	0.438
C	6.899	6.701	0.920	1.025	6.489	1.143	2.064	0.409
D	6.955	6.756	1.116	1.254	6.540	1.393	0.277	0.414
E	6.834	6.633	0.763	0.887	6.420	1.013	0.250	0.414

3.3. Ionization potential (IP) and electronic affinity (EA)

It is known that a balanced charge carrier injection/transport will improve the charge recombination efficiency and hence enhance the efficiency of OLEDs. Herein, ionization potentials (IP), electron affinities (EA), reorganization energy (λ), hole and electron extraction potential (HEP and EEP) have been calculated and shown in Table 2. The details definitions for these physical quantities can be obtained from many literatures [40,41]. It can be seen that the IP value of complex **B** is the smallest one, which means that the hole injection is much easier in complex **B** than others. The EA value of complex **D** is the largest, which means the electron injection is much easier than the other complexes. A small IP (large EA) means that the holes (electrons) are easy to inject into emitter from the anode (cathode); thus the turn-on voltage is low and the performance of devices is good. Therefore, the hole-injection abilities for **B** and **D** are improved, while the electron-injection abilities will be decreased. In addition, one can find that complexes **A** and **C** have the best hole transfer abilities with the smallest λ_{hole} value (0.409 eV) among these complexes. As shown in Table 2, the $\lambda_{electron}$ value for complex **C** are obviously larger than the λ_{hole} value, which suggests that the hole transfer rate is better than the electron transfer rate. It can be seen that the difference between $\lambda_{electron}$ and λ_{hole} for complex **D** is the smallest among these complexes, which can greatly improve the charge transfer balance, thus further enhancing the device performance of OLEDs.

3.4. Absorption spectra

On the basis of the optimized ground state geometries, the absorption properties of complexes **A**–**E** were calculated using the

TDDFT/B3LYP method. The vertical electronic excitation energies, oscillator strengths (f), assignment, and configurations are listed in Table S6 (Supporting information). The absorption spectra of the studied complexes in CH_2Cl_2 medium based on the TDDFT calculations are shown in Fig. 3.

The lowest energy absorption wavelengths are located at 378 nm (f=0.0219) for **A**, 430 nm (f=0.0124) for **B**, 411 nm (f=0.0239) for **C**, 436 nm (f=0.0124) for **D**, and 394 nm (f=0.0149) for **E**. The calculated lowest lying absorption 378 nm for **A** is comparable to the experimental values 363 nm [32]. It can be seen that the lowest energy absorption wavelengths and oscillator strengths for complexes **B** and **D** are very close or identical, which shows the similar intramolecular energy transfer characters. Fig. 3 shows that complexes **A**–**E** have the similar absorption shapes at 275 nm wavelength except **C** with the two weak split peaks. For all these complexes studied, the lowest lying absorptions are attributed to the HOMO→LUMO transition with more than 96% composition and the character of MLCT (singlet metal to ligand charge transfer)/LLCT (singlet ligand-to-ligand charge transfer) [d(Ir)+π(bdp)→π*(N^N)], which can be interpreted as the charge transfer transition from the Ir(III) metal center and the bdp auxiliary ligand to the cyclometalating ligand moiety based upon the molecular orbital composition analysis. In addition, it can also be seen that the incorporation of the N atom leads to an obvious redshift of the peak absorption for **B**, **C**, **D**, and **E** with respect to that of complex **A**. The calculated vertical triplet absorptions of complexes **A**–**E** are at 410, 454, 436, 462, and 416 nm (Table S6, Supporting information), respectively, having the d(Ir)+π(bdp)→π*(N^N)/MLCT/ILCT transition characters.

For a better analysis of the excited state's nature, the natural transition orbital (NTO) based on TDDFT/B3LYP has been analyzed to assist the assignment of the electronic transition [42,43]. The occupied NTO can be seen as the "hole" orbital (i.e., the orbital from which electron is removed during transition), whereas "virtual" NTO is the orbital in which electron is placed in the excited state. The plots of the occupied and virtual NTOs correspond to electronic transitions from the ground state to the singlet excited states S_1 and are shown in Fig. 4. It is also noted that NTO analysis confirms the MLCT/LLCT nature of the $S_0 \rightarrow S_1$ transition. All the complexes **A**–**E** have the similar occupied orbitals and virtual orbitals. The occupied orbitals are mainly localized on Ir(III) atom and the benzyldiphenylphosphine auxiliary ligand. The virtual orbitals are equally localized on the portions of two main ligands.

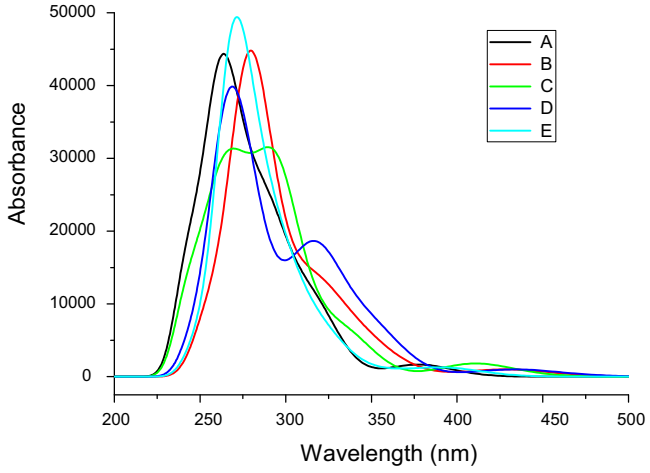

Fig. 3. Simulated absorption spectra in CH_2Cl_2 medium for complexes **A**, **B**, **C**, **D**, and **E**.

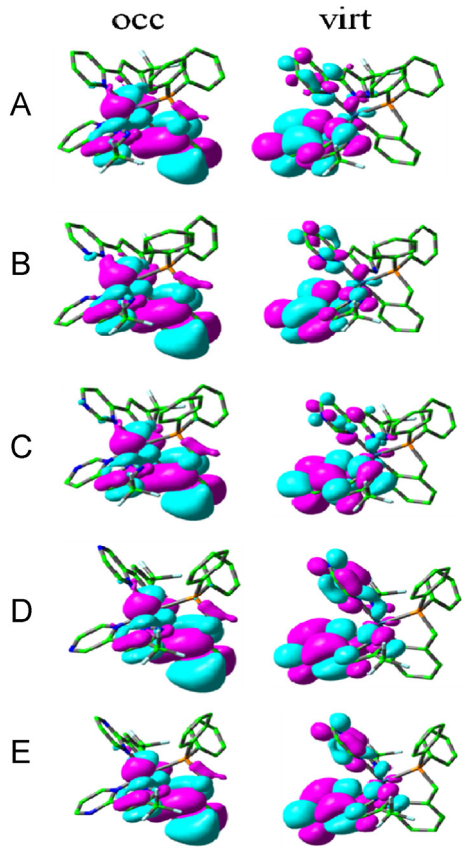

Fig. 4. The plots of the occupied and virtual NTOs corresponding to electronic transitions from the ground state to the singlet excited state S_1.

3.5. Phosphorescence

To check the computational method, two different density functionals (CAM-B3LYP and M052X) were used [44,45]. A good agreement with the experimental data was obtained for M052X, while a disagreement was found for CAM-B3LYP. The calculated lowest energy emissions for **A**–**E** at M052X level are localized at 450, 409, 438, 483, and 429 nm, respectively. For **A**, the lowest energy emission at M052X (450 nm) is in good agreement with the experimental data (461 nm) [32]. On the basis of the optimized T_1 structures, the emission wavelengths, emission energies, and transition nature of complexes **A**–**E** calculated by the TDDFT/M052X method in CH_2Cl_2 medium have been listed in Table 3. The partial compositions of frontier molecular orbitals (FMOs) related to emission have also been presented in Table S7 (Supporting information) to analyze the transition property of emission. In addition, the plots of the molecular orbitals related to emissions of **A**–**E** are presented in Fig. 5. It can be seen that the calculated lowest energy emissions of complexes **A**–**E** are localized at 450 nm (2.75 eV), 409 nm (3.02 eV), 438 nm (2.82 eV), 483 nm (2.56 eV), and 429 nm (2.88 eV), respectively. The calculated lowest energy emission of **A** is in good agreement with the experimental data 461 nm [32]. It is obvious that there is a blue-shift for complexes **B**, **C**, and **E** compared to **A**, while a relatively larger redshift is observed for complex **D**. Table 3 shows that the lowest energy emissions of complexes **A**–**E** originate from different transitions and characters. For example, complex **E** has the L→H-3 (36%) and L→H (28%) transitions assigned to [π*(N^N)→d(Ir)+π(N^N+bdp)] with the mixed characters of ^{3}MLCT(triplet metal to ligand charge transfer)/^{3}LLCT(triplet ligand-to-ligand charge transfer). It is well-known that a large Ir d orbital

Table 3
Phosphorescent emissions of **A**, **B**, **C**, **D**, and **E** in CH_2Cl_2 medium at the TDDFT/M052X levels, respectively, along with experimental wavelength (nm) available. (H indicates HOMO, and L indicates LUMO).

	λ(nm)/E(eV)	Configuration	Nature	Exptl.[a]
A	450/2.75	L→H-2(64%)	π*(N^N)→π(N^N+bdp)/^{3}LLCT	461
		L→H(19%)	π*(N^N)→d(Ir)+π(N^N+bdp)/^{3}MLCT/^{3}LLCT	
B	409/3.02	L→H(48%)	π*(N^N)→d(Ir)+π(N^N+bdp)/^{3}MLCT/^{3}LLCT	
		L→H-4(15%)	π*(N^N)→d(Ir)+π(N^N)/^{3}MLCT/^{3}LLCT	
C	438/2.82	L→H(58%)	π*(N^N)→d(Ir)+π(N^N+bdp)/^{3}MLCT/^{3}LLCT	
		L→H-3(14%)	π*(N^N)→d(Ir)+π(N^N+bdp)/^{3}MLCT/^{3}LLCT	
D	483/2.56	L→H-2(47%)	π*(N^N)→d(Ir)+π(N^N+bdp)/^{3}LLCT	
		L→H-3(24%)	π*(N^N)→d(Ir)+π(N^N+bdp)/^{3}LLCT	
E	429/2.88	L→H-3(36%)	π*(N^N)→d(Ir)+π(N^N+bdp)/^{3}MLCT/^{3}LLCT	
		L→H(28%)	π*(N^N)→d(Ir)+π(N^N+bdp)/^{3}MLCT/^{3}LLCT	

[a] From Ref. [32]

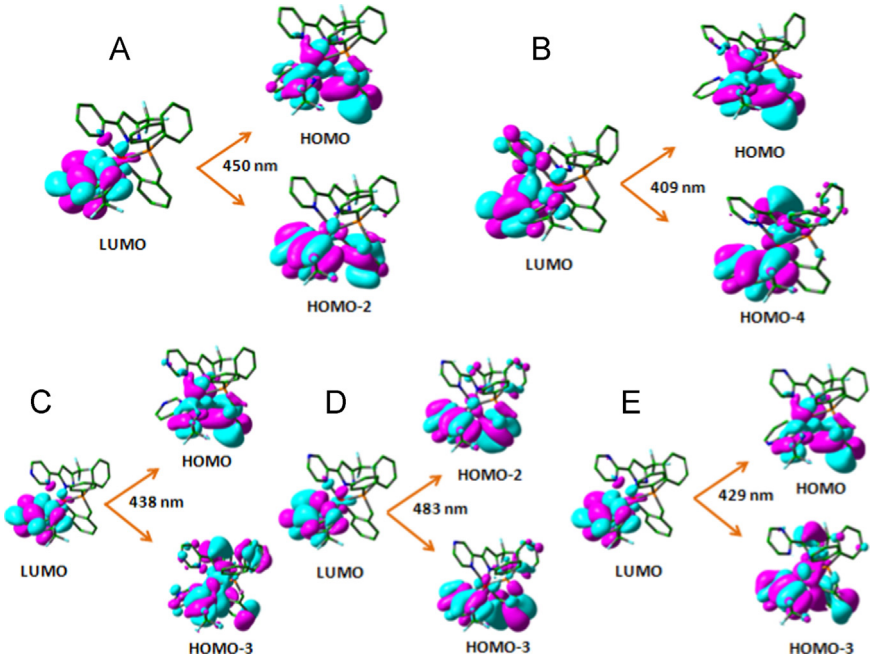

Fig. 5. Transitions responsible for the emissions at 450, 409, 438, 483, and 429 nm for complexes **A**, **B**, **C**, **D**, and **E**, respectively, simulated in CH_2Cl_2 medium at the TDDFT/M052X levels.

contribution in HOMOs is beneficial for the high ^{3}MLCT composition and consequently increases the transition probability. The partial molecular orbital composition (%) of complexes **A**–**E** in the triplet excited states in Table S7 shows a large contribution from Ir d orbitals to HOMOs (30–32%) for the studied complexes except complex **D**, resulting in substantial metal–ligand mixing with the π-orbitals of the N^N and bdp ligands. The PPh_2 unit and the non-conjugated cyclometalating benzyl group would exert the greatest ligand field stabilization energy as well as the largest π–π* energy gap among all the established chelates. From the discussions above, it can be seen that the N substitution may be a very good method to tune the emitting color of complex **A**.

3.6. Phosphorescence quantum efficiency

The emission quantum yield (Φ) can be affected by the competition between k_r (radiative decay rate) and k_{nr} (nonradiative decay rate), i.e. $\Phi = k_r/(k_r + k_{nr})$. It can be seen, to increase the quantum yield, k_r should be increased and k_{nr} should be decreased simultaneously or respectively [46,47]. In addition, k_r is also theoretically related to the mixing between S_1 and T_1, which is proportional to the spin-orbit coupling (SOC) and inversely proportional to the energy gaps between the S_1 and T_1 states according to the following formula [48,49]:

$$k_r \approx \gamma \frac{\langle \psi_{S_1} | H_{S_0} | \psi_{T_1} \rangle^2 \mu_{S_1}^2}{(\Delta E_{S_1 - T_1})^2} \quad (1)$$

$$\gamma = 16\pi^3 10^6 n^3 E_{em}^3 / 3h\varepsilon_0$$

where H_{S_0} is the Hamiltonian for the spin-orbit coupling, μ_{S_1} is the transition dipole moment in the $S_0 \rightarrow S_1$ transition, $\Delta E_{S_1 - T_1}$ is the energy gaps between the S_1 and T_1 states [50,51], E_{em} represents the emission energy in cm^{-1} and n, h, and ε_0 are the refractive index, Planck's constant and the permittivity in a vacuum, respectively. Accordingly, the variation of quantum yield (Φ) can be qualitatively analyzed in theory from the above formula.

It is known that the phosphorescence quantum efficiencies could be increased by a larger ^{3}MLCT composition and thus the intersystem crossing (ISC). For iridium atom, the direct involvement of the d(Ir) orbital enhances the first-order SOC in the $T_1 \rightarrow S_0$ transition and thus ISC, which would result in a drastic decrease of the radiative lifetime and avoid the nonradiative process [52]. In Table 4, we have listed the ^{3}MLCT contributions which were calculated to be 10.7%, 14.2%, 16.8%,

Table 4
The contribution of ^{3}MLCT (%) in the T_1 state and the energy gaps between the S_1 and T_1 states ($\Delta E_{S_1-T_1}$) (in eV), along with the transition electric dipole moment in the $S_0 \rightarrow S_1$ transition μ_{S_1}, the radiative decay rate k_r ($\times 10^5\ s^{-1}$) and nonradiative decay rate k_{nr} ($\times 10^5\ s^{-1}$), together with the observed quantum yields Φ [%] and lifetime τ for complex **A** in CH_2Cl_2 medium.

	^{3}MLCT	$\Delta E_{S_1-T_1}$	μ_{S_1}	Φ[a]	τ[a]
A	10.7	0.27	0.27	0.005	0.01
B	14.2	0.16	0.17		
C	16.8	0.29	0.32		
D	8.7	0.20	0.17		
E	13.1	0.25	0.19		

[a] Ref. [32]

8.7%, and 13.1% for complexes **A–E**, respectively. It can be seen that **D** has the smallest ^{3}MLCT contribution among these complexes studied. It is also known that the phosphorescence quantum efficiencies are inversely proportional to the $\Delta E_{S_1-T_1}$ [53]. Namely, a minimal $\Delta E_{S_1-T_1}$ is required for enhancing the ISC rate, leading to the increased k_r. $\Delta E_{S_1-T_1}$ for these complexes are listed in Table 4, along with the μ_{S_1} values. The results give 0.27, 0.16, 0.29, 0.20, and 0.25 eV for $\Delta E_{S_1-T_1}$, respectively for **A–E**. From the discussion above, it is obvious that the lower $\Delta E_{S_1-T_1}$ the larger ^{3}MLCT contribution and higher μ_{S_1} value may account for a larger k_r according to Eq. (1). From the data in Table 4, it can be seen that the complex **C** has possibly the larger k_r value than those of other complexes.

4. Conclusions

The geometrical and electronic structures, absorption and emission spectra, charge injection and transport abilities, and phosphorescence efficiency of five Ir(III) complexes have been investigated by the DFT and TDDFT methods, discussing the effect a systematic substitution of the "CH" group by the electron-withdrawing nitrogen (N) atom on the photophysical properties. Complex **D** possibly possesses the best charge transfer balance among these complexes studies. The calculated absorption and emission properties of complex **A** have a good agreement with the available experimental data. In addition, the absorption and emission properties for these complexes show substantial difference in terms of the different N atom substitution. The calculated results show that complex **C** possibly possesses the largest radiative decay rate (k_r) value among these complexes studied. This study would be useful to provide guidance for the design and synthesis of novel phosphorescent transition metal complex used in OLEDs.

Acknowledgments

The authors are grateful to the financial aid from the Program of Science and Technology Development Plan of Jilin Province of China (Grant nos. 20140520090JH, and 20130206032YY) and the funds for Doctoral Scientific Research Startup of Changchun University of Science and Technology (Grant no. 40301855).

Appendix A. Supporting information

Supplementary data associated with this article can be found in the online version at http://dx.doi.org/10.1016/j.jlumin.2014.10.064.

References

[1] M.S. Lowry, W.R. Hudson, R.A. Pascal, S. Bernhard, J. Am. Chem. Soc. 126 (2004) 14129.
[2] A.B. Tamayo, S. Garon, T. Sajoto, P.I. Djurovich, I.M. Tsyba, R. Bau, M.E. Thompson, Inorg. Chem. 44 (2005) 8723.
[3] S.W. Thomas, K. Venkatesan, P. Müller, T.M. Swager, J. Am. Chem. Soc. 128 (2006) 16641.
[4] F.C. Hsu, Y.L. Tung, Y. Chi, C.C. Hsu, Y.M. Cheng, M.L. Ho, P.T. Chou, S.M. Peng, A.J. Carty, Inorg. Chem. 45 (2006) 10188.
[5] V.L. Whittle, J.A.G. Williams, Inorg. Chem. 47 (2008) 6596.
[6] R.D. Costa, F.J. Céspedes-Guirao, E. Ortí, H.J. Bolink, J. Gierschner, F. Fernández-Lázaro, A. Sastre-Santos, Chem. Commun. 26 (2009) 3886.
[7] F. Kessler, Y. Watanabe, H. Sasabe, H. Katagiri, M.d.K. Nazeeruddin, M. Grätzel, J. Kido, J. Mater. Chem. C 1 (2013) 1070.
[8] X.B. Xu, X.L. Yang, J.S. Dang, G.J. Zhou, Y. Wu, H. Li, W.Y. Wong, Chem. Commun. 50 (2014) 2473.
[9] S. Lamansky, P. Djurovich, D. Murphy, F.A. Razzaq, H.E. Lee, C. Adachi, P.E. Burrows, S.R. Forrest, M.E. Thompson, J. Am. Chem. Soc. 123 (2001) 4304.
[10] C. Adachi, R.C. Kwong, P. Driovich, V. Adamovich, M.A. Baldo, M.E. Thompson, S.R. Forrest, Appl. Phys. Lett. 79 (2001) 2082.
[11] X.H. Shang, Y.Q. Liu, X.C. Qu, Z.J. Wu, J. Lumin. 143 (2013) 402.
[12] H.J. Bolink, E. Coronado, S.G. Santamaria, M. Sessolo, N. Evans, C. Klein, E. Baranoff, K. Kalyanasundaram, M. Graetzel, M.K. Nazeeruddin, Chem. Commun. (2007) 3276.
[13] J. Ding, B. Wang, Z. Yue, B. Yao, Z. Xie, Y. Cheng, L. Wang, X. Jing, F. Wang, Angew. Chem. Int. Ed. 48 (2009) 6664.
[14] V.K. Rai, M. Nishiura, M. Takimoto, Z. Hou, Chem. Commun. 47 (2011) 5726.
[15] K.S. Yook, J.Y. Lee, Adv. Mater. 24 (2012) 3169.
[16] G. Tan, S. Chen, N. Sun, Y. Li, D. Fortin, W.Y. Wong, H.S. Kwok, D. Ma, H. Wu, L. Wang, P.D. Harvey, J. Mater. Chem. C 1 (2013) 808.
[17] M.A. Baldo, D.F. O'Brien, Y. You, A. Shoustikov, S. Sibley, M.E. Thompson, S.R. Forrest, Nature 395 (1998) 151.
[18] C. Adachi, M.A. Baldo, S.R. Forrest, M.E. Thompson, Appl. Phys. Lett. 77 (2000) 904.
[19] S. Lamansky, P. Djurovich, D. Murphy, F. Abdel-Razzaq, H.E. Lee, C. Adachi, P.E. Burrows, S.R. Forrest, M.E. Thompson, J. Am. Chem. Soc. 123 (2001) 4304.
[20] W.Y. Wong, C.L. Ho, Coord. Chem. Rev. 253 (2009) 1709.
[21] R.J. Holmes, S.R. Forrest, Y.J. Tung, R.C. Kwong, J.J. Brown, S. Garon, M.E. Thompson, Appl. Phys. Lett. 82 (2003) 2422.
[22] S.J. Su, E. Gonmori, H. Sasabe, J. Kido, Adv. Mater. 20 (2008) 4189.
[23] Y. Zhen, S.H. Eom, N. Chopra, J. Lee, F. So, J. Xue, Appl. Phys. Lett. 92 (2008) 223301.
[24] F.M. Hwang, H.Y. Chen, P.S. Chen, C.S. Liu, Y. Chi, C.F. Shu, F. Wu, P.T. Chou, S.M. Peng, G.H. Lee, Inorg. Chem. 44 (2005) 1344.
[25] J. Li, P.I. Djurovitch, B.D. Alleyene, M. Yousufudin, N.N. Ho, J.C. Thomas, J.C. Peters, R. Bau, M.E. Thompson, Inorg. Chem. 44 (2005) 1713.
[26] K. Dedeian, J. Shi, N. Shepherd, E. Forsythe, D.C. Morton, Inorg. Chem. 44 (2005) 4445.
[27] G.J. Zhou, C.L. Ho, W.Y. Wong, Q. Wang, D.G. Ma, L.X. Wang, Z.Y. Lin, T.B. Marder, A. Beeby, Adv. Funct. Mater. 18 (2008) 499.
[28] S.C. Lo, R.E. Harding, C.P. Shipley, S.G. Stevenson, P.L. Burn, I.D.W. Samuel, J. Am. Chem. Soc. 131 (2009) 16681.
[29] Y.C. Chiu, J.Y. Hung, Y. Chi, C.C. Chen, C.H. Chang, C.C. Wu, Y.M. Cheng, Y.C. Yu, G.H. Lee, P.T. Chou, Adv. Mater. 21 (2009) 2221.
[30] J.Y. Hung, Y. Chi, I.H. Pai, Y.M. Cheng, Y.C. Yu, G.H. Lee, P.T. Chou, K.T. Wong, C.C. Chen, C.C. Wu, Dalton Trans. (2009) 6472.
[31] Y.C. Chiu, Y. Chi, J.Y. Hung, Y.M. Cheng, Y.C. Yu, M.W. Chung, G.H. Lee, P.T. Chou, C.C. Chen, C.C. Wu, H.Y. Hsieh, ACS Appl. Mater. Interfaces 1 (2009) 433.
[32] Y.C. Chiu, J.Y. Hung, Y. Chi, C.C. Chen, C.H. Chang, C.C. Wu, Y.M. Cheng, Y.C. Yu, G.H. Lee, P.T. Chou, Adv. Mater. 21 (2009) 2221.
[33] P. Hohenberg, W. Kohn, Phys. Rev. 136 (1964) B864.
[34] A.D. Becke, J. Chem. Phys. 98 (1993) 5648.
[35] C. Lee, W.T. Yang, R.G. Parr, Phys. Rev. B 37 (1988) 785.
[36] P.J. Hay, W.R. Wadt, J. Chem. Phys. 82 (1985) 270.
[37] P.J. Hay, W.R. Wadt, J. Chem. Phys. 82 (1985) 299.
[38] N.M. O'Boyle, A.L. Tenderholt, K.M. Langner, J. Comput. Chem. 29 (2008) 839.
[39] M.J. Frisch, G.W. Trucks, H.B. Schlegel, G.E. Scuseria, M.A. Robb, J.R. Cheeseman, G. Scalmani, V. Barone, B. Mennucci, G.A. Petersson, H. Nakatsuji, M. Caricato, X. Li, H.P. Hratchian, A.F. Izmaylov, J. Bloino, G. Zheng, J.L. Sonnenberg, M. Hada, M. Ehara, K. Toyota, R. Fukuda, J. Hasegawa, M. Ishida, T. Nakajima, Y. Honda, O. Kitao, H. Nakai, T. Vreven, J.A. Montgomery, Jr., J.E. Peralta, F. Ogliaro,M. Bearpark, J.J. Heyd, E. Brothers, K.N. Kudin, V.N. Staroverov, R. Kobayashi, J. Normand, K. Raghavachari, A. Rendell, J.C. Burant, S.S. Iyengar, J. Tomasi, M. Cossi, N. Rega, J.M. Millam, M. Klene, J.E. Knox, J.B. Cross, V. Bakken, C. Adamo, J. Jaramillo, R. Gomperts, R.E. Stratmann, O. Yazyev, A.J. Austin, R. Cammi, C. Pomelli, J.W. Ochterski, R.L. Martin, K. Morokuma, V.G. Zakrzewski, G.A. Voth, P. Salvador, J.J. Dannenberg, S. Dapprich, A.D. Daniels, J.B. Foresman, J.V. Ortiz, J. Cioslowski, D.J. Fox, Gaussian 09, Gaussian, Inc., Wallingford CT, 2009.
[40] R.A. Marcus, Rev. Mod. Phys. 65 (1993) 599.
[41] R.A. Marcus, J. Chem. Phys. 24 (1956) 966.
[42] R.L. Martin, J. Chem. Phys. 118 (2003) 4775.
[43] J.D. Chai, M. Head-Gordon, Phys. Chem. Chem. Phys. 10 (2008) 6615.
[44] T. Yanai, D.P. Tew, N.C. Handy, Chem. Phys. Lett. 393 (2004) 51.
[45] E.G. Hohenstein, S.T. Chill, C.D. Sherrill, J. Chem. Theory Comput. 4 (2008) 1996.

[46] S. Fantacci, F. De Angelis, A. Sgamellotti, A. Marrone, N. Re, J. Am. Chem. Soc. 127 (2005) 14144.
[47] A.B. Tamayo, S. Garon, T. Sajoto, P.I. Djurovich, I.M. Tsyba, R. Bau, M.E. Thompson, Inorg. Chem. 44 (2005) 8723.
[48] S. Haneder, E. Da Como, J. Feldmann, J.M. Lupton, C. Lennartz, P. Erk, E. Fuchs, O. Molt, I. Munster, C. Schildknecht, G. Wagenblast, Adv. Mater. 20 (2008) 3325.
[49] N. Turro, Modern Molecular Photochemistry, University Science Books, Palo Alto, CA, 1991.
[50] P.J. Hay, J. Phys. Chem. A 106 (2002) 1634.
[51] A.R.G. Smith, M.J. Riley, S.C. Lo, P.L. Burn, I.R. Gentle, B.J. Powell, Phys. Rev. B: Condens. Matter Mater. Phys. 83 (2011) 041105.
[52] C.H. Yang, Y.M. Cheng, Y. Chi, C.J. Hsu, F.C. Fang, K.T. Wong, P.T. Chou, C.H. Chang, M.H. Tsai, C.C. Wu, Angew. Chem. Int. Ed. 46 (2007) 2418.
[53] I. Avilov, P. Minoofar, J. Cornil, L.De Cola, J. Am. Chem. Soc. 129 (2007) 8247.